Evaluation of blast effects on a civilian/industrial structure in the case of a scenario of a terrorist attack involving improvised explosive devices (IEDs)

Cristian Rădeanu[1*], *Denisa* Tudor[2], *Ilie-Ciprian* Jitea[1], *Ladislau* Radermacher[2], and *Attila* Kovacs[1]

[1]National Institute for Research and Development in Mine Safety and Protection to Explosion – INSEMEX Petroşani Department of Safety Explosives and Pyrotechnic Aticles, 32 34 G-ral Vasile Milea St., 332047 - Petroşani, Hunedoara County, Romania
[2] University of Petrosani, Hunedoara County, Romania

Abstract. In recent decades, the risk of attacks within operational and neutral zones has increased considerably. A significant proportion of these attacks are executed using improvised explosive devices (IEDs), which are non-conventional weapons that can be assembled with relative ease. There is growing concern about the possibility that a kamikaze might self-detonate when armed forces or law enforcement agencies discover the location where they are preparing their materials or are simply inside a building. To study the possible effects these improvised explosive devices (IEDs) would have on structures, eight tests were conducted with various IED configurations involving bomb vests inside a reinforced concrete building (including walls and roof) specifically built for these tests. These vests were made with different explosives (black powder, ANFO, AN/AL, PG2). To characterize these tests, a high-speed camera and pressure and acceleration sensors were used. The structure performed surprisingly well, as it withstood all of the first seven detonations without apparent structural damage. In the final detonation, located on the ground and with a significant explosive charge, the structural integrity of the roof and some of the walls was compromised. The building simulation was carried out using the LS-DYNA software, with a Lagrangian formulation for the walls, using the LBE module (based on CONWEP) for load application. Despite the difficulty of this simulation, the results obtained, in terms of applied pressures and measured accelerations, are acceptable, with differences of approximately 20%.

1 Introduction

Most IED attacks recorded over the past 15 years have involved small explosive charges of less than 5 kg, or person-borne devices typically containing under 10 kg of explosives.

* Corresponding author: cristian.radeanu@insemex.ro

IED attacks are frequently conducted in crowded public areas, urban environments, in proximity to critical infrastructure, or even inside buildings. Accordingly, there has been an increased focus on the structural damage caused by such explosions and their effects on built environments [1]. This has led to a growing body of literature dedicated to blast mitigation strategies and structural retrofitting techniques. However, a substantial portion of these studies rely predominantly on numerical modelling rather than experimental validation. Such models are often calibrated using empirical equations or, in some cases, validated against limited experimental data available in the literature [2]. Given the evolving threat landscape, further research is required to deepen the understanding of victimization risks associated with blast overpressure and fragmentation effects, particularly when explosive devices are detonated within enclosed building environments.

Since concrete is a widely used construction material in many building structures, its behaviour has been extensively studied through experimental testing and numerical simulation. For these reasons, many experiments focus on individual structural elements, such as beams or slabs, which are easier to handle and monitor [3,4]. The failure of individual structural elements can have a decisive influence on whether or not the structure collapses. Progressive collapse of structures has also been studied by numerous researchers, although few have conducted large-scale experimental tests, and even fewer have included non-structural elements such as masonry walls or roofs along with the structure itself [5,6].

This paper presents the results of computer-based simulations of various test scenarios involving different IED configurations detonated inside a building with a composite concrete structural system. As part of this research, eight tests were conducted using different IED configurations simulating a PBIED inside a building using vest bombs. The building consisted of a small concrete structure measuring 6.80 x 5 meters, with a corridor and an interior room. This study focuses on the analysis of high-speed video recordings, the pressures and accelerations recorded during the tests, and the development of a suitable numerical model capable of reproducing the behaviour of blast effects inside the building.

2 Test description and instrumentation

The structure built ad hoc for the tests was made of reinforced concrete and consisted of a perimeter corridor and an interior room in which the improvised explosive devices were placed. The initial idea was to use brick enclosures, but these would have been destroyed after each trial, making the project unfeasible in terms of both time and cost. For this reason, the structure was redesigned with reinforced concrete walls, with greater thickness for the exterior walls than for the interior ones. The doors and windows were also aligned to improve the venting of the shock wave. The floor plan dimensions of the structure are shown in Figure 1, with the height between the floor and the ceiling of the structure being 3 meters. The exterior walls were built with a thickness of 40 cm, while the interior walls had a thickness of 30 cm, and the roof slab was 25 cm thick. The concrete used for both the walls and the roof slab had a nominal compressive strength of 40 MPa, a density of 2300 kg/m³, a tensile strength of 3.5 MPa, a modulus of elasticity of 30.9 GPa, and a maximum aggregate size of 20 mm. The reinforcement of the structure, made of ribbed steel B-500 C, was distributed equally on both sides of the walls and on the roof slab in both directions (vertical and horizontal). The vertical reinforcement steel of the exterior walls was made using 12 mm diameter rebar, evenly spaced at 300 mm, while in the interior walls, the rebar used had a diameter of 10 mm, spaced at 200 mm. The horizontal steel in the exterior walls had a diameter of 8 mm, spaced at 150 mm; although the same diameter was used in the interior walls, the spacing was increased to 200 mm. The roof reinforcement was arranged symmetrically on both sides, inside the cube where the detonation took place and, on the outside, using 12 mm diameter rebars with a 150 mm square mesh on each side. In height,

both reinforcements were spaced 180 mm apart, with the slab thickness being 250 mm; therefore, a sufficient concrete cover was ensured on both sides. Finally, there was perimeter reinforcement at all joints between the walls and the roof, using 16 mm diameter rebars, vertically spaced at 160 mm. It was assumed that the steel had a density of 7850 kg/m³, a Young's modulus of 200 GPa, a yield strength of 500 MPa, a Poisson's ratio of 0.3, and a tangent modulus of 20 GPa, according to EN 1992-1-1:2004 [7] and EN 1998-2:2:2005 [8]. Lastly, the floor of the structure was covered with a 15 cm thick reinforced concrete layer with a #15 x 15 x 6 steel mesh.

Eight tests were carried out (Table 1), and a preliminary (trial) detonation was conducted to verify the operation of the measuring and recording equipment installed in the area. The explosives used in the tests were black powder, ANFO, AN/AL, and PG-2 (similar to US C-4). The black powder used has a composition of potassium nitrate (75%), sulphur (10%), and carbon (15%), and is always granulated and graphitized, with particle sizes ranging from 0.1 to 4 mm. ANFO (ammonium nitrate and fuel oil) is the stoichiometric mixture of ammonium nitrate and fuel oil. AN/AL consists of a mixture of ammonium nitrate and aluminium powder. Finally, PG-2 is a military explosive whose composition is mainly RDX embedded in plastic additives.

The IEDs created for these tests were attached to different types of personal vests and, in some cases, were confined to steel tubes. The design of the explosive charges used in each test was based on the quantities of each type of explosive that can be included in a typical suicide vest configuration: in tests T1–T6 (black powder, ANFO, and AN/AL), the explosives were placed inside steel tubes, while in tests T7 and T8 (plastic explosive – PG2), the charges were attached directly to the inside of the vest. In all tests involving vests and tubes (tests T1–T6), 0.7 meters of 15 g/m detonating cord were used to initiate the main charge. In contrast, in the tests where the explosive was directly attached to the vest (without tubes – T7 and T8), 3.7 meters of detonating cord were used. It should be noted that the mass of explosive in test T8 is higher than the PG2 equivalent, as the remaining charges were included.

The test instrumentation consisted of accelerometers, pressure sensors, recording equipment, and a high-speed camera. Figure 1 shows the placement of the pressure sensors (P1 and P2), the accelerometers (A1–A5), and the two recording devices used (DT1 and DT2).

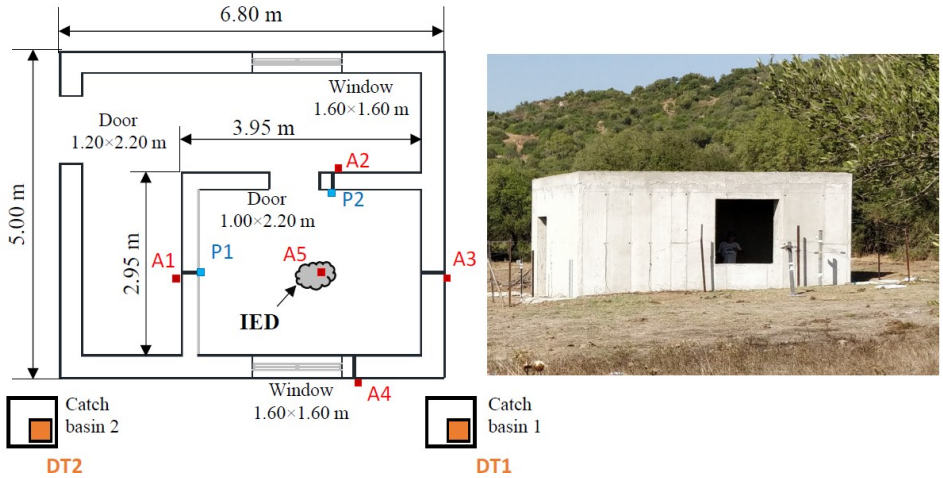

Fig.1. Details of the structure, placement of the measuring equipment, and photograph of the structure. The letters P refer to pressure sensors, the letters A indicate accelerometers, and DT refers to Datatrap II recording equipment.

Table 1. Loading characteristics during the tests performed.

Test	Type of explosive	Charge (kg)	PETN (g)	TNT equivalent mass (kg)	Enclosure
T0	PG-2	0.10	0	0.14	–
T1	Black powder	3.37	10.5	0.79	Steel tubes
T2	Black powder	3.27	10.5	0.77	Steel tubes
T3	ANFO	2.29	10.5	1.48	Steel tubes
T4	ANFO	2.20	10.5	1.42	Steel tubes
T5	AN/AL	2.16	10.5	1.88	Steel tubes
T6	AN/AL	2.25	10.5	1.95	Steel tubes
T7	PG-2	7.00	55	9.87	Vest
T8	PG-2	8.20	55	14.21	Vest

The two pressure sensors used were PCB 5000 PSI (344.7 MPa), model 102B, equipped with ablative protection for the fireball. The sensors were placed through a passage tube in the concrete wall, so that the sensing surface was perpendicular to the main direction of impact. In this way, the first recorded wave would be the one reflected from the wall where the sensor was installed. These sensors were positioned at a height of 1.51 m and 1.55 m for P1 and P2, respectively. Piezoelectric PCB shock accelerometers were used, placed on the opposite side of the wall from the explosive charge, with a measurement limit of 5,000 or 10,000 g (Table 2). In the accelerometer position labelled A1, one sensor was used for tests T0–T4 and a different one for the last three tests (T5–T7), due to the sensor being damaged during test T4. In the final test (T8), no measuring equipment was used due to the risk of complete destruction of the structure or, at the very least, compromising its structural stability. It is worth noting that the sensor located at position A5 was placed on the roof of the structure, outside of it (Figure 1). Two Datatrap II recorders from MREL were used for data acquisition. See Figure 2 for more details regarding the measuring equipment and their positions.

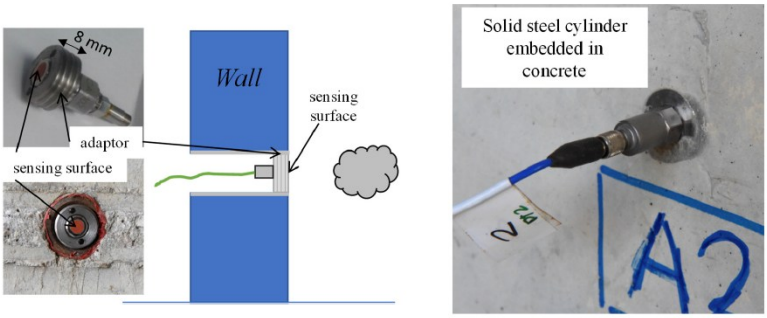

a) b)

Fig.2. Details (a) Pressure sensors (PCB 102B), details of P1. (b) Accelerometer in position A2.

Table 2. Loading characteristics during the tests performed

#Sensor	Model	Measurement range (g)	Test	Height (m)
A1	350C23	±10,000	T0–T4	1.375
A1	350C04	±5000	T5–T7	1.375
A2	350C04	±5000	T0–T7	1.370
A3	350C23	±10,000	T0–T7	1.395
A4	350B04	±5000	T0–T7	1.370
A5	350B04	±5000	T0–T7	3.300

Finally, the high-speed camera (HSC) used was a Photron Fastcam SA3-120k, adapted for blast testing with a steel housing (Figure 3). It reaches a recording speed of 5,000 frames per second at a resolution of 512 x 512 pixels, and up to 120,000 fps at a resolution of 128 x 16 pixels.

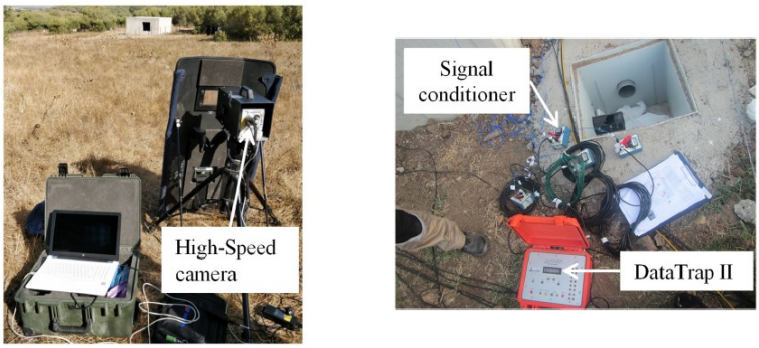

a) (b)

Fig.3. Details (a) Placement of the high-speed camera in one of the tests. (b) Signal conditioners and DataTrap II recording equipment.

3 Numerical model

The 3D numerical models were developed using the LS-DYNA software, version 971-R11 [9], which is based on explicit numerical methods suitable for solving problems involving large deformations subjected to explosions. The computer used for these simulations had two Intel XEON E5-2630 v4 processors at 2.20 GHz (10 cores each, 2 threads per core), with 64 GB of RAM and a Windows 10 operating system.

Acceleration in LS-DYNA can be measured using sensors at specific coordinates [10]. Processing this data is sometimes complex and generally does not work well when the blast is modelled using tabular values, such as with the Load Blast_Enhanced (LBE) command. An alternative approach is to use the Database_History Node command to explicitly track the history of a specific node's characteristics (e.g., acceleration, velocity, displacement, etc.).

3.1 Finite element model

This model consisted of two main critical parts: concrete and steel reinforcement. In addition, the ground was also included in the model, but only for visualization purposes (Figure 4). The "Constrained Lagrange in Solid" functionality was used to ensure the correct interaction of both materials as a single assembly. This option can be applied because the interaction between the components (steel and concrete) can be assumed to be ideal, given that the event is nearly instantaneous [11]. Furthermore, the structure was anchored to the ground using a Single Point Constraint (SPC), eliminating displacements and rotations in all spatial directions.

The concrete was defined using 3D Lagrangian solid elements with reduced integration to minimize computation time. The element size used for the concrete was 20 mm, based on previous studies on the response of concrete to blasting under similar conditions and loading. The reinforcement was modelled using beam-type elements with a length of 50 mm. The number of solid elements was 5,150,187, while the number of beam elements was 64,266 [12].

Fig.4. Details (a) Placement of the high-speed camera in one of the tests. (b) Signal conditioners and DataTrap II recording equipment.

3.2 Blast implementation

The implementation of the explosive charge can be approached in two different ways: by using the parameters of the explosive material and its equation of state [4]; or by using a TNT equivalent for the charge and implementing it with the Load Blast Enhanced (LBE) function. The latter option is usually simpler to implement and more computationally efficient, while still producing very good results.

The For the load application in this case, LBE was used, which is the method through which LS-DYNA introduces CONWEP. This can be used under the assumption that the steel tubes might have a lethal effect on people but are relatively harmless to the structure [13]. With the LBE instructions, the input parameters required to calculate and apply the generated pressure (both incident and reflected) on the concrete elements are: the type of shock wave, the TNT equivalent mass, the coordinates of the charge centre, and the concrete surfaces where the pressure wave will be applied. The software applies pressures according to Friedlander's equation to compute the pressure curve, including the negative phase. Additionally, pressures were recorded only in the room where the improvised explosive devices were placed. Therefore, pressures were applied via LBE only to all faces of that room (including the ceiling), and not outside of it, such as in the corridor.

3.3 Materials

LS-DYNA offers more than 25 models that can be used to describe concrete, some requiring many input parameters, while others operate with minimal data, though not all perform well under blast conditions. In this research, the CSCM (Continuous Surface Cap Model) was used to describe the behaviour of concrete. The automatic generation of parameters was based on the input of compressive strength, maximum aggregate size, and density. This model operates with isotropic elastic behaviour prior to cracking, transitioning to a plastic behaviour limited by failure surfaces. The model includes an internal damage calculation that allows element erosion when they reach 99% of the damage limit, and the maximum principal strain in the element exceeds a user-defined value, known as ERODE [14]. The material properties used in this model are presented in Table 3.

Table 3. Properties of the concrete and steel used in the numerical modelling

Property	Concrete	Steel
Density (kg/m³)	2300	7850
Uniaxial compressive strength (MPa)	40	-
Maximum aggregate size (m)	0.02	-
Young's modulus (MPa)	-	2×10^5
Poisson's ratio	-	0.3
Yield stress (MPa)	-	5×10^2
Tangent modulus (MPa)	-	2×10^4

The steel used for reinforcement was the standard B-500 S, introduced into the model as a “Piecewise Linear Plasticity” material model [15]. In this study, failure was defined based on the effective plastic strain, as opposed to failure determined by the timestep of the numerical model through convergence of the method. The value entered was 0.075, meaning that when the plastic strain reaches this value, the element is removed from the calculation [12].

4 Results and discussion

4.1 High-speed camera

The images were captured at a speed ranging between 3000 and 5000 fps. If in the T2 test where black powder was used in steel tubes, the powder generated a significant volume of gases that were expelled practically simultaneously through the two openings to the outside of the cabin, it was possible to compare the images of the test using gunpowder with those recorded in the test (T4) where ANFO was used, and important differences were observed in terms of the expansion of the fireball and the volume of gases generated. The fireball did not reach the exterior in the case of the ANFO test, and the volume of gases was significantly lower. Figure 5 presents a sequence of 12 images obtained in a test with AN/AL (T6). The fireball expanded considerably more than in the ANFO test due to the aluminium in its composition.

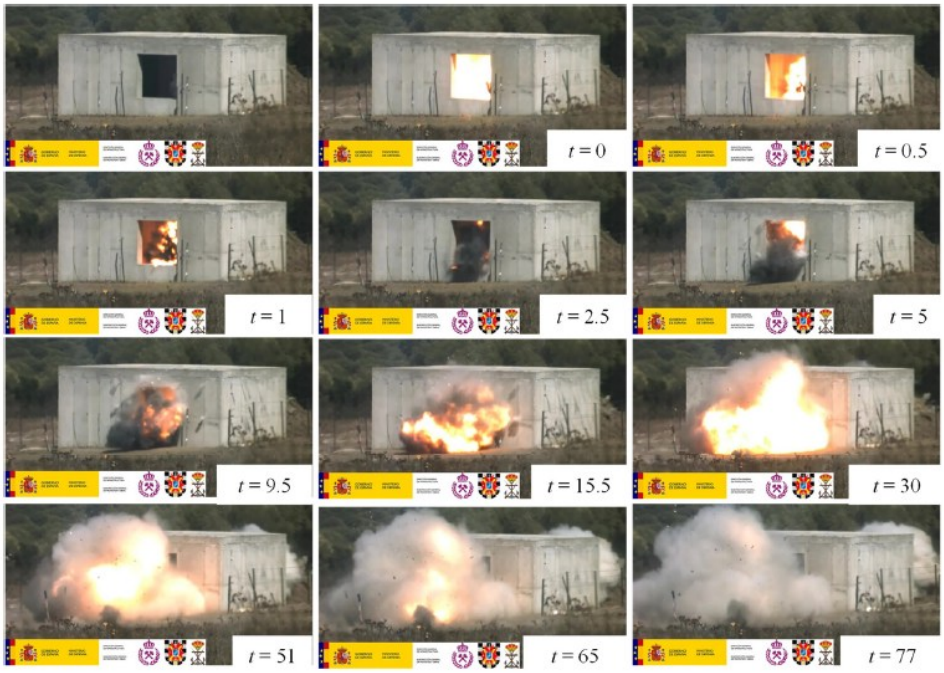

Fig.5. Sequence of images captured with the HSC during test T6: AN/AL. Time in milliseconds; the reference time is the first video frame showing the detonation.

Figure 6 shows a similar sequence of images from test T7, involving the detonation of a vest (without steel tubes) loaded with 7 kg of PG2 plastic explosive. The expansion of the fireball fully reaches the facade on both the front and rear sides of the cabin. The first images

taken immediately after the initiation of the detonation reveal a large white glow, indicating extremely high temperatures.

Fig.6. Sequence of images captured with the HSC during test T7: PG2. Time in milliseconds; the reference time is the first video frame showing the detonation.

4.2 Pressure signals

In some cases, the recording of different pressure–time signals exhibited a significant level of noise that could mask the actual signal. In such cases, signal filtering is necessary to extract the shock wave parameters. Pressure measurements were recorded with reasonable reliability in tests T0 to T2 (see Table 4). The simulation values are compared with the average field values when more than one signal is available. See Figure 7 as an example of pressure application.

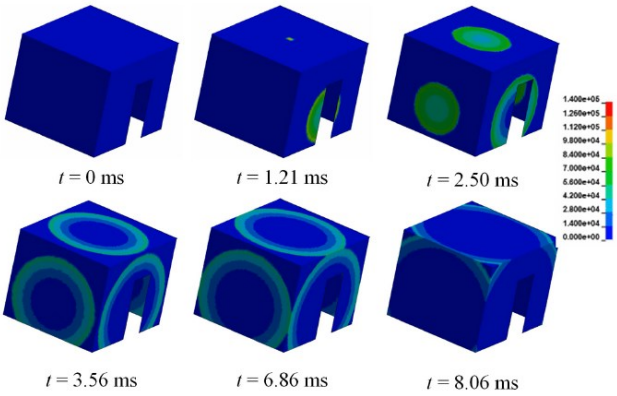

Fig.7. Pressure values (view from the inner door) on the interior surfaces of the room where the detonations were carried out for test T0. The colour scale represents pressure values in Pa.

The sequence shows how the wave first reaches the inner wall of the door (the area closest to the IED), then the ceiling. It then reaches the rest of the surfaces and expands in a very similar manner.

As shown in Table 4, the values simulated with the LBE card are quite close to those obtained in the field, with relatively low errors considering the nature of the phenomenon. The results show differences of approximately 11%, which indicates that the simulation is relatively reliable and that the TNT equivalent used in describing the explosives was fairly accurate.

Table 4. Pressure sensor results. Friedlander fitting

Test	Explosive	Sensor	P_r (kPa)	P_r (LS-DYNA) (kPa)	Relative Dif. (%)
T0	PG-2	P1	88.72	99.67	−12.34
T0	PG-2	P2	129.80	136.02	−4.79
T1	Black Powder	P1	193.11	181.21	6.71
T2	Black Powder	P1	195.38		
T1	Black Powder	P2	372.27	309.64	17.93
T2	Black Powder	P2	382.36		

Acceleration Figure 8 illustrates how the LBE simulation reproduces only the first peak of the signal recorded by the sensors. Moreover, the pressures recorded by sensor P1 are significantly lower—nearly half—compared to those recorded by sensor P2. This may be due to the orientation of the explosive device, which was more directly focused toward P2, with no direct "line of sight" to the sensor located at P1. However, the multiple reflections acting on the sensor are greater at P1, which makes sense given that it is farther from the large openings represented by the doors and windows.

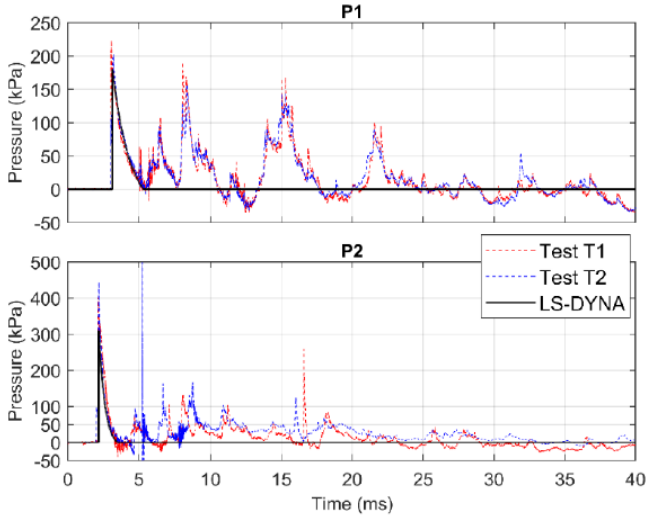

Fig.8. Pressure signals (P1 and P2) for tests T1 and T2: black powder and the simulated signal with LS-DYNA.

4.3 Acceleration signals

The peak acceleration values comparing all simulations and measurements from the different sensors (A1–A4, Figure 1 and Table 2) can be found in Table 5. Sensors that were not measured in the field are not included in Table 5, which is intended to show the differences between the measured and simulated values.

Table 5. Peak acceleration values for different sensors and tests. PB stands for black powder

Test	Explosive	#Sensor	Measured Acceleration (g)	Model Acceleration (g)	Difference (%)
T0	PG2	A2	44.4	26.3	40.77
		A3	77.1	57.8	25.03
		A4	29.6	30.2	−1.94
T1	BP	A1	207.2	152.8	26.25
		A3	699.3	416.5	40.44
		A4	69.2	79.9	−15.49
T2	BP	A1	105.2	75.4	28.30
		A3	430.3	403.6	6.21
		A5	298.8	354.8	−18.76
T3	ANFO	A1	1048.9	852.4	18.73
T4	ANFO	A1	1113.6	928.3	16.64
		A3	1048.2	809.9	22.74
		A4	259.8	349.4	−34.50
		A5	1646.4	1056.0	35.86
T5	AN/AL	A1	998.9	1115.2	−11.64
		A3	3786.5	4192.0	−10.71
		A4	4685.5	4896.0	−4.49
		A5	2683.10	1691.5	36.96
T6	AN/AL	A1	903.4	1126.5	−28.68
		A3	5600.6	4305.0	23.13
		A4	4828.6	5094.0	−5.50
		A5	1996.25	1518.4	23.94
T7	PG2	A1	902.7	652.0	27.77
		A3	1507.90	1521.8	3.12
		A4	5171.8	3464.4	33.01
		A5	1342.3	1505.0	−12.12

As shown in Table 5 for sensors A1 through A4, the recorded acceleration values are quite high for the ANFO, AN/AL, and PG2 tests, ranging between 1000 and 5000 g, while in the black powder tests, the acceleration values are around 400 g. This clearly indicates that accelerations increase with the use of more powerful charges, as expected. Given the nonlinear nature of the phenomenon, as well as the inherent limitations of the simulation itself, the differences between the model and the actual data are fairly reasonable, with an average absolute error of 20%. Therefore, the model can reproduce acceleration peaks with a certain level of reliability. The largest discrepancy is found in the only valid measurement from sensor A2 and from sensor A3 in test T1. On the other hand, the smallest error is observed again at sensor A3 in test T7, followed by sensor A4 in tests T5 and T6. The highest average values are recorded by sensor A1, but with the smallest deviations. Based on these results, it can be concluded that the differences between measured and simulated values are most significant at sensor A1.

Overall, the model is able to reproduce the field measurements with average (and absolute) errors of approximately 25%. Therefore, in this test, the timing of the acceleration peaks in LS-DYNA and in the experimental test does not match, although the peak values themselves are consistent.

Despite the increase in explosive charge, the peak accelerations recorded on the roof decreased slightly, unlike those recorded by the other sensors. This was particularly noticeable in test T7, which involved 7 kg of PG2. The sensor A5, located on the roof of the structure (see Figure 1), shows somewhat different results (see Table 5 and Figure 9). This may be a consequence of reduced structural stiffness due to accumulated damage from conducting the tests consecutively, without intermediate reinforcement or any structural support interventions. It is possible that the additional stiffness provided by the double reinforcement used in the roof slab lost its effectiveness after so many tests, although it was likely what prevented an earlier collapse of the structure.

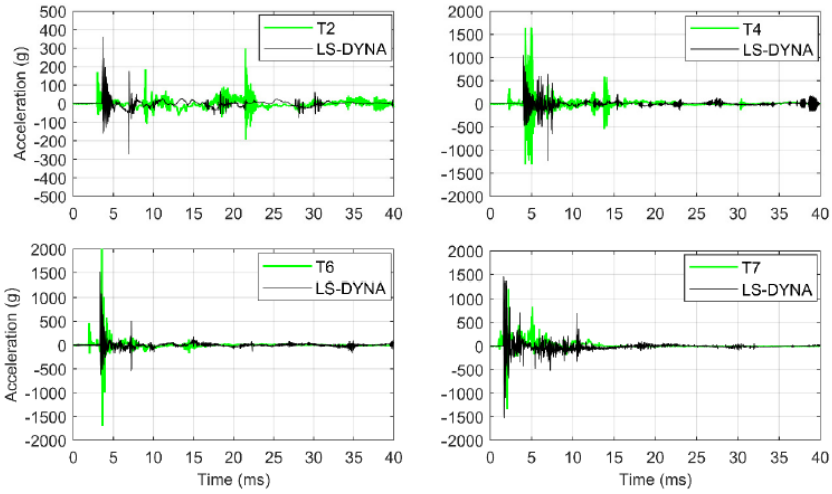

Fig.9. Pressure Accelerations from tests T2, T4, T6, and T7 at position A5 (see Figure 1) and their comparison with LS-DYNA.

Supporting this idea, the model (Figure 10) clearly shows stress concentrations around the window and at the joints between the roof slab and the walls—areas that therefore endured the highest stress levels throughout the tests. The image sequence shows that within two seconds, the stresses within the structure had already stabilized. It can also be observed that after test T7, the stress state of the structure is considerably higher than before.

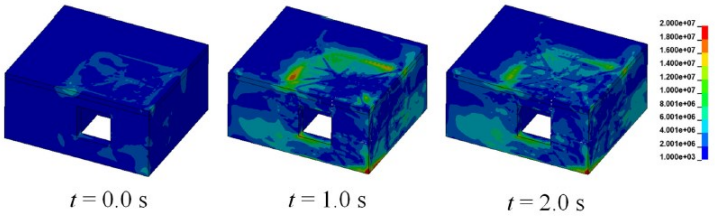

Fig.10. Effective stress (scale in Pa) from test T7. The first image at time zero corresponds to the stress state at the moment the T7 test charge is detonated in the model.

4.4 Final Test T8

Figure 11 shows the condition of the structure after the final test (T8).

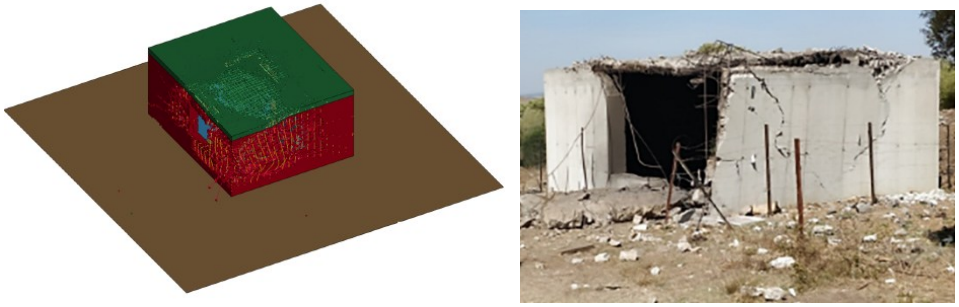

Fig.11. Effective Results of the final test (T8): numerical model and photograph

In this test, the explosive charge was placed on the ground in the corner between the access door wall and the location of sensor P1 (see Figure 1). It can be observed that the structure was destroyed along the window wall and the adjacent wall on the DT1 side (see Figure 1). The gases attempted to escape through that area (as seen in the previous test, T7, in Figure 5), projecting most of the shock wave energy onto this already weakened part of the structure. As a result, the walls and part of the roof collapsed, leaving the reinforcement exposed. In the model, something similar occurs: although the roof appears to be slightly more damaged than in the real structure, the side wall shows significant damage, just as it did during the test.

4.5 Effects of the type of improvised explosive device

The results show that the improvised explosive devices (IEDs) used in the tests (T1–T6), in which relatively low-power explosives with small charges were confined in tubes, can generate high accelerations. These pressures are undoubtedly caused by the confinement of the explosive inside a steel tube, as an airburst detonation would likely produce milder effects. This confinement leads to greater structural damage due to the higher accelerations involved. See Figure 12 for details on the interior parts of the structure affected by successive detonations.

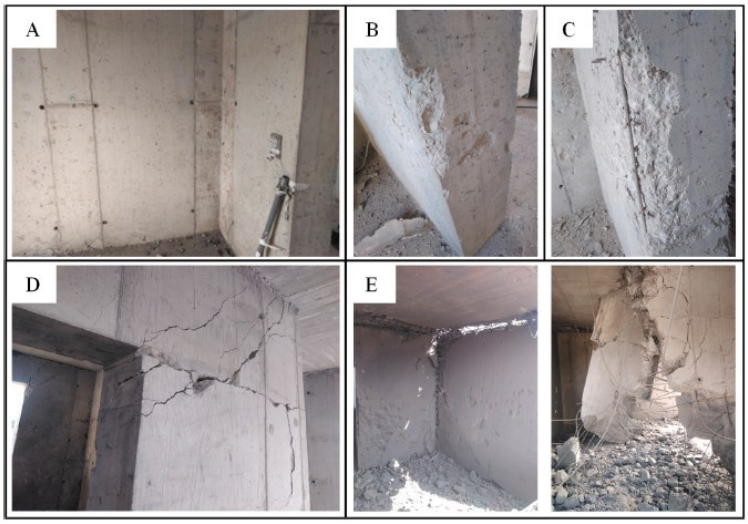

Fig.12. Different effects of improvised explosive devices on the interior structure: (A) after the two black powder tests (T1–T2); (B) after the ANFO tests (T3–T4); (C) after the AN/AL tests (T5–T6); (D) after the first PG2 test (T7); (E) after the second PG2 test (T8).

It can be observed that the black powder tests have very little impact on the structure or the concrete (Figure 12A). In the case of ANFO, which is a more powerful charge, some chipping of the concrete can be seen near the inner door (Figure 12B). The same occurs with AN/AL, where the first layers of reinforcement become visible, indicating that erosion was already significant (Figure 12C). The case of the plastic explosive (T7-T8) is slightly different, as it is a very powerful explosive that does not need confinement to improve its performance, producing significant damage to the structure, as observed in the cracks generated in the inner wall (Figure 12D). As mentioned earlier, in the final test (T8), the charge was much larger, which resulted in the roof becoming detached from the walls (Figure 12E), in addition to the evident collapse that occurred near the exterior window area.

5 Conclusions

A total of eight tests were carried out using different types of improvised explosive devices on the same reinforced concrete structure, simulating a scenario in which charges are detonated upon security forces entering the building. The following conclusions can be drawn:

- High-speed camera footage allows us to visually confirm the proper detonation of the explosive, while the pressure log enables validation of the model's input data;
- Acceleration recorded at the roof level of the structure decreases as more tests are conducted, due to the loss of structural stiffness;
- IEDs with relatively low power (using homemade explosives or low-TNT equivalents), although they generate significant accelerations within the structure, do not compromise its structural stability, whereas higher-power IEDs (plastic explosives), even with similar acceleration levels, pose a risk to the structural integrity of the building;
- A solid-element model using LBE provides, even in complex scenarios such as this, a reasonably accurate reproduction of structural behaviour, helping reduce testing costs by allowing different scenarios to be simulated with a certain degree of confidence.

”This work was carried out through the ”Nucleu” Program within the National Plan for Research, Development and Innovation 2022-2027, with the support of the Romanian Ministry of Education and Research – National Authority for Research, project no. 23 32 02 03, title: Development of monitoring methods to reduce environmental impact from the use of explosive materials, pyrotechnic articles, and application of blasting technologies.
(in Romanian: Aceasta lucrare a fost realizata prin Programul-Nucleu din cadrul Planului National de Cercetare Dezvoltare si Inovare 2022-2027, derulat cu sprijinul MEC-ANC, proiect nr. 23 32 02 03, titlu: Dezvoltarea metodelor de monitorizare în vederea reducerii impactului de mediu în urma utilizarii materialelor explozive, articolelor pirotehnice si aplicarii tehnologiilor de împuscare)”.

References

1. Sielicki, P.W.; Stewart, M.G.; Gajewski, T.; Peksa, P.; Al-rifaie, H.; Studzi, R. Field Test and Probabilistic Analysis of Irregular Steel Debris Casualty Risks from a Person-Borne Improvised Explosive Device. Def. Technol. **2021**, 17, 1852–1863.
2. Tai, Y.S.; Chu, T.L.; Hu, H.T.;Wu, J.Y. Dynamic Response of a Reinforced Concrete Slab Subjected to Air Blast Load. Theor. Appl. Fract. Mech. **2011**, 56, 140–147.
3. Zhao, C.; Lu, X.; Wang, Q.; Gautam, A.; Wang, J.; Mo, Y.L. Experimental and Numerical Investigation of Steel-Concrete (SC) Slabs under Contact Blast Loading. Eng. Struct. **2019**, 196, 109337.
4. Daniela Reifarth, C.; Castedo, R.; Santos, A.P.; Chiquito, M.; López, L.M.; Pérez-Caldentey, A.; Martínez-Almajano, S.; Alañon, A. Numerical and experimental study of externally reinforced RC slabs using FRPs subjected to close-in blast loads. Int. J. Impact Eng. **2021**, 156, 103939.
5. Bermejo, M.; Santos, A.P.; Goicolea, J.M. Development of Practical Finite Element Models for Collapse of Reinforced Concrete Alshaikh, I.M.H.; Bakar, B.H.A.; Alwesabi, E.A.H.; Akil, H. Experimental Investigation of the Progressive Collapse of Reinforced Concrete Structures: An Overview. Structures **2020**, 25, 881–900.
6. Stewart, M.G.; Mueller, J. Terrorism Risks, Chasing Ghosts and Infrastructure Resilience. Sustain. Resilient Infrastruct. **2020**, 5, 78–89.

7. EN 1992-1-1; Eurocode 2: Design of Concrete Structures—Part 1-1: General Rules and Rules for Buildings. European Committee for Standardization: Brussels, Belgium, 2004.
8. EN 1998-2; Eurocode 8: Design of Structures for Earthquake Resistance—Part 2: Bridges. European Committee for Standardization: Brussels, Belgium, 2005.
9. Livermore Software Technology Corporation (LSTC). LS-DYNA Keyword User´s Manual—R11; Livermore Software Technology Corporation: Livermore, CA, USA, 2018; p. 3186.
10. Castedo, R.; Segarra, P.; Alañon, A.; Lopez, L.M.; Santos, A.P.; Sanchidrian, J.A. Air Blast Resistance of Full-Scale Slabs with Different Compositions: Numerical Modeling and Field Validation. Int. J. Impact Eng. **2015**, 86, 145–156.
11. Castedo, R.; Santos, A.P.; Alañón, A.; Reifarth, C.; Chiquito, M.; López, L.M.; Martínez-Almajano, S.; Pérez-Caldentey, A. Numerical Study and Experimental Tests on Full-Scale RC Slabs under Close-in Explosions. Eng. Struct. **2021**, 231, 111774.
12. Alañón, A.; Cerro-Prada, E.; Vázquez-Gallo, M.J.; Santos, A.P. Mesh Size Effect on Finite-Element Modeling of Blast-Loaded Reinforced Concrete Slab. Eng. Comput. **2018**, 34, 649–658.
13. Abedini, M.; Zhang, C. Performance Assessment of Concrete and Steel Material Models in LS-DYNA for Enhanced Numerical Simulation, A State of the Art Review. Arch. Comput. Methods Eng. **2021**, 28, 2921–2942.
14. Brad, D.; Michael, O.; Joseph, M. Modeling Reinforced Concrete Protective Construction for Impact Scenarios. In Proceedings of the International Explosives Safety Symposium and Exhibition, San Diego, CA, USA, 6–9 August 2018; p. 298.
15. Cadoni, E.; Dotta, M.; Forni, D.; Tesio, N. High Strain Rate Behaviour in Tension of Steel B500A Reinforcing Bar. Mater. Struct. Constr. **2015**, 48, 1803–1813.